


Article

A High Thermal Conductivity of MgO-H₂O Nanofluid Prepared by Two-Step Technique

Hadia Kadhim Judran ¹, Adnan G. Tuaamah Al-Hasnawi ¹, Faten N. Al Zubaidi ¹,
Wisam Abed Kattea Al-Maliki ^{2,3} , Falah Alobaid ^{3,*}  and Bernd Eppe ³

¹ Electromechanical Engineering Department, University of Technology-Iraq, Baghdad 19006, Iraq; 50100@uotechnology.edu.iq (H.K.J.); 10597@uotechnology.edu.iq (A.G.T.A.-H.); 50241@uotechnology.edu.iq (F.N.A.Z.)

² Mechanical Engineering Department, University of Technology-Iraq, Baghdad 19006, Iraq; wisam.a.kattea@uotechnology.edu.iq

³ Institut Energiesysteme und Energietechnik, TU Darmstadt, Otto-Berndt-Straße 2, 64287 Darmstadt, Germany; bernd.eppe@est.tu-darmstadt.de

* Correspondence: falah.alobaid@est.tu-darmstadt.de

Abstract: In this paper, the main goal is to study the impact of nanopowder volume concentration and ultrasonication treatment time on the stability and thermophysical properties of MgO-DW nanofluid at room temperature. The co-precipitation method was utilized to prepare pure MgO nanoparticles with an average particle size of 33 nm. The prepared MgO nanopowder was characterized by using XRD, SEM, and EDX analyses. Then, MgO-DW nanofluid was obtained with different volume concentrations (i.e., 0.05, 0.1, 0.15, 0.2, and 0.25 vol.%) and different ultrasonication time periods (i.e., 45, 90, 135, and 180 min) by using a novel two-step technique. With volume concentration and ultrasonication time of 0.15 vol.% and 180 min, respectively, good stability was achieved, according to the zeta potential analysis. With increasing volume concentration and ultrasonication time period of the nanofluid samples, the thermal conductivity measurements showed significant increases. As a result, the maximum enhancement was found to be 25.08% at a concentration ratio of 0.25 vol.% and agitation time of 180 min. Dynamic viscosity measurements revealed two contrasting trends with volume concentration and ultrasonication time. The lowest value of relative viscosity was gained by 0.05 vol.% MgO-DW nanofluid. The chemical and physical interactions between MgO nanoparticles and DW molecules play an important function in determining the thermal conductivity and dynamic viscosity of MgO-DW nanofluid. These findings exhibit that MgO-DW nanofluid has the potential to be used as an advanced heat transfer fluid in cooling systems and heat exchangers.

Keywords: MgO-DW nanofluid; two-step technique; co-precipitation; XRD and SEM; thermal conductivity; dynamic viscosity



Citation: Judran, H.K.; Al-Hasnawi, A.G.T.; Al Zubaidi, F.N.; Al-Maliki, W.A.K.; Alobaid, F.; Eppe, B. A High Thermal Conductivity of MgO-H₂O Nanofluid Prepared by Two-Step Technique. *Appl. Sci.* **2022**, *12*, 2655. <https://doi.org/10.3390/app12052655>

Academic Editor: Jianzhong Lin

Received: 10 January 2022

Accepted: 2 March 2022

Published: 4 March 2022

Publisher's Note: MDPI stays neutral with regard to jurisdictional claims in published maps and institutional affiliations.



Copyright: © 2022 by the authors. Licensee MDPI, Basel, Switzerland. This article is an open access article distributed under the terms and conditions of the Creative Commons Attribution (CC BY) license (<https://creativecommons.org/licenses/by/4.0/>).

1. Introduction

High thermal conductivity fluids are referred to as nanofluids and are employed rather than regular fluids to increase heat transfer properties or to prevent overheating. Numerous studies have demonstrated that standard fluids used in heat exchangers, such as water, oil, ethylene glycol, and glycerol, have low thermal conductivity as compared with metallic and ceramic materials [1–3]. Therefore, praiseworthy attempts have been made to improve the thermal conductivity of traditional fluids, by distributing ultrafine solid particles. The growing requirement for high efficiency in heat exchangers, storage materials in electronic devices, chemical reactions, boiling processes, and solar energy has prompted researchers to focus on dispersed particles, particularly within a size range of 1–100 nm, within the base fluid [4–9].

Maxwell [10,11] was the first to conduct practical research to increase heat conductivity, and he was supported by a large number of researchers. Among the most prominent, Choi,

suggested the concept of blending nanoparticles into traditional working fluids to enhance the thermophysical properties and heat transfer characteristics of the working fluids.

Choi formulated the idiom “nanofluid” at the Argonne National Laboratory in the United States of America in 1995 [12]. Nanofluids have unique and effective features such as larger specific surface area (SSA) nanoparticles, high suspension stability (longer suspension time), reduced erosion of ducts, significant energy saving, minimal viscosity increase, and higher heat transfer rate as compared with the milli- and micro-sized suspension fluids proposed by Maxwell [13,14]. Therefore, different aspects of nanofluids have been studied such as synthesis techniques [15–17], thermophysical properties such as thermal conductivity and dynamic viscosity [18–23], and nanofluid applications [16,24]. Because of its clear influence on heat transfer, thermal conductivity is worth investigating. Accordingly, researchers have worked hard to investigate aspects that have an impact on thermal conductivity, such as the shape (morphology) and size of the dispersed phase (nanopowder), type of the base fluid, temperature, synthesis technique, using or not using and type of surfactant (additives), pH, nanopowder concentration, and ultrasonication time [25–30]. Metal oxide nanopowders are widely used in nanofluid preparation due to their chemical stability as compared with metals, as well as their good thermal conductivity, abundance, and cheapness [31,32]. Metal oxide nanoparticles such as MgO, CuO, Al₂O₃, ZnO, TiO₂, Fe₂O₃, and SiO₂ are suitable candidates for the development of effective heat transfer fluids due to their significant properties. Among these particles, MgO has played a critical role in improving the thermal properties of traditional fluids. In addition, MgO nanofluid has been employed in various applications including catalysis, catalyst supports, nuclear reactors, storage materials, and boiling processes [33–37].

Subsequently, investigators have extensively examined MgO nano oxides. Various physical and chemical methods have been used for preparation of MgO nanopowder, involving vapor deposition [38], co-precipitation [39,40], sol-gel [41,42], molecular beam epitaxial [43], spray pyrolysis [44], ultrasonic irradiation [45], microwave irradiation [46], hydrothermal [39], plasma irradiation [47], surfactant methods [48], combustion method [49], solvothermal [50], and thermal evaporation [51], in addition to biological sterilization methods [52], such as fungal strain *Aspergillus terreus* [53], and so-called green synthesis [54,55]. Although MgO nanopowder can be prepared via the different previously mentioned approaches, the co-precipitation method has several advantages due to its simplicity, effectiveness, high surface area of the nano product, and economic route [56]. There are two major techniques that can be used to synthesize nanofluid, i.e., single-step and two-step techniques. Nevertheless, in terms of a two-step procedure, any of the aforementioned methods can synthesize MgO nanofluid. In both techniques, applying the ultrasonication treatment is the pivotal operator for breaking down the agglomerated nanoparticles to attain a high stable nanofluid [4]. Thermal conductivity and viscosity of the MgO/propylene glycol nanofluid were extensively improved by S. Manikandan and K. S. Rajan [57] at various MgO nanopowder concentrations (0–2 vol.%), temperatures (20–60 °C), and ultrasonication times (0–30 h). Firstly, MgO nanopowder with an average particle size of 35 nm was prepared by a simple chemical reaction route. Then, a two-step technique was devoted to synthesizing the nanofluid using probe ultrasonication for 25 h. The average thermal conductivity enhancement was 20% for 2 vol.% MgO/propylene glycol nanofluid and was detected to be independent of temperature. The relative viscosity of the nanofluid was decreased with nanoparticle concentration at a temperature of 30 °C. At a higher ultrasonication time, both thermal conductivity and viscosity were clearly improved with ultrasonication time up to 0.243 (W/M·°K) and 25 (mPa·sec), respectively. M. H. Esfa et al. [58] prepared MgO nanofluid by suspending nanoparticles (40 nm) in a binary base fluid of water and ethylene glycol (60:40) using a two-step technique. In this technique, an ultrasonication treatment time of up to 4 h was applied. The impact of different solid concentrations and different temperatures were investigated. The results showed that the thermal conductivity of MgO/H₂O-EG nanofluid increased with an increase in nano MgO volume concentration and temperature. Using a two-step technique, a hybrid

nanofluid of Ag-MgO/water was also conducted by the M. H. Esfa research group [5]. The nanofluid was produced by mixing 25 nm nano Ag (50%), 40 nm nano MgO (50%), and water. Ultrasonic vibration for 3 h and CTAB surfactant were employed to ensure better stability.

Thermal conductivity and dynamic viscosity were measured as a function of nanoparticle volume fraction range between 0% and 2%. The obtained results revealed that both thermal conductivity and dynamic viscosity were increased with increases in the volume fraction of (Ag + MgO) nanoparticles. The effects of particle size, solid concentration, and temperature on the dynamic viscosity of ethylene glycol-based nanofluid containing MgO nanoparticles have been studied by K. Yapici et al. [59]. They conducted experiments at concentrations ranging from 5 to 20 wt.% of MgO nanopowder with particle sizes of 20 and 40 nm. MgO/EG nanofluid was agitated in an ultrasonic bath for 6 h by using a two-step technique. Nonlinear results revealed that the 20 nm and 40 nm MgO nanoparticles exhibited non-Newtonian behavior at weight concentrations higher than 5%. J. Lu et al. [60] used molten salt $\text{LiNO}_3\text{-NaNO}_3\text{-KNO}_3$ with MgO nanoparticles to prepare nanofluid via a two-step technique. The synthesis technique was concluded by heating the mixture of molten salt and MgO nanoparticles to 350 °C and ultrasonication time for 1 h. The effect of nanoparticles on thermal properties was studied with different sizes ranges of 20–100 nm, weight concentrations from 0.5 to 2.0 wt.%, and temperature. The results showed that the enhancement of thermal conductivity of salt with 1 wt.% nano-MgO could be 5.3–11.7%. In an experimental environment, S. R. Nfawa et al. [61] improved the thermal conductivity of a CuO-MgO/H₂O hybrid nanofluid in an experimental setting. The hybrid nanofluid was synthesized and investigated at various volume fractions (i.e., 0.125–1.25%) of 80% CuO and 20% MgO nanoparticles which were dispersed in water at temperatures ranging from 25 to 50 °C. The zeta potential measurement indicated that the 0.25% (CuO-MgO)/H₂O hybrid nanofluid had a good stability of −45.1 mV. The study results showed that by increasing the concentration ratio, the CuO-MgO/H₂O hybrid nanofluid's thermal conductivity was clearly enhanced; however, this enhancement began to decline when the concentration was higher than 1 vol.% as a result of nanoparticle precipitation.

The two-step approach is often supported by the aid of relatively high temperatures, and/or the use of surfactants, and/or a long ultrasonication treatment time, and/or organic base fluids. Therefore, in the present study, we aimed at preparing MgO-DW nanofluid with efficient thermal properties such as better stability, high thermal conductivity, and low viscosity, without using surfactants or stabilizers, and with environmentally friendly nanofluid at room temperature.

Furthermore, the plurality of the concerned investigations has been considered in order to exploit MgO nanopowder as an additive or to synthesize hybrid nanofluid with other nanomaterials, as cited in [62–66]. However, in this work, pure MgO-DW nanofluid was produced with functional properties. This was achieved by using MgO nanopowder with a unique morphology of feathery or fluffy-like nanostructure, while usually, the nano shape used in nanofluid preparation is spherical particles. The abovementioned aspects are all assumed to be novel, making MgO-DW nanofluid an excellent alternative for heat transfer applications.

2. Experimental Details

2.1. Materials and Method

The co-precipitation method was used to create MgO nanopowder. Analytical grade chemicals such as magnesium sulfate ($\text{MgSO}_4 \cdot 7\text{H}_2\text{O}$), sodium bicarbonate (NaHCO_3), ammonium hydroxide (NaOH), and sodium dodecyl sulfate (SDS) were utilized without additional purification. NaOH and SDS were both used as a surfactant at room temperature. The chemicals used were all from BDH Chemicals Ltd., Poole, Dorset, UK. First, a 0.8 M solution of NaHCO_3 and NaOH was prepared by dissolving a suitable quantity in deionized water. Similarly, Mg precursor solution was prepared by dissolving $\text{MgSO}_4 \cdot 7\text{H}_2\text{O}$ in deionized water. Next, 50 mL of 0.5 M MgSO_4 and SDS solution were blended fully by

stirring vigorously by utilizing a magnetic stirrer for 20 min at room temperature. Then, using a burette, 50 mL of 0.8 M NaHCO_3 solution was gently poured into it, while it was constantly stirred. Then, 50 mL of 1 M NaOH solution was added in batches into the above resulting solution under stirring. The final combination was left to swirl for 4 h after adding the surfactant and precipitating agent, with no parameters being modeled.

The extremely finely powdered white precipitate MgO was collected at the bottom of the preparation flask once the time was up. The fine powder was carefully separated using a centrifuge. The whole precipitation was washed several times with distilled water. The main purpose of the washing process was to ensure that the precipitate was free from foreign trace elements, especially SDS residue. The resulting MgO powder was dried in an air oven at 60°C for 2 h. Then, the prepared MgO nanopowder was produced via a calcination process using a furnace at 350°C for 1 h. All details of the preparation method are explained in Figure 1 (first step).

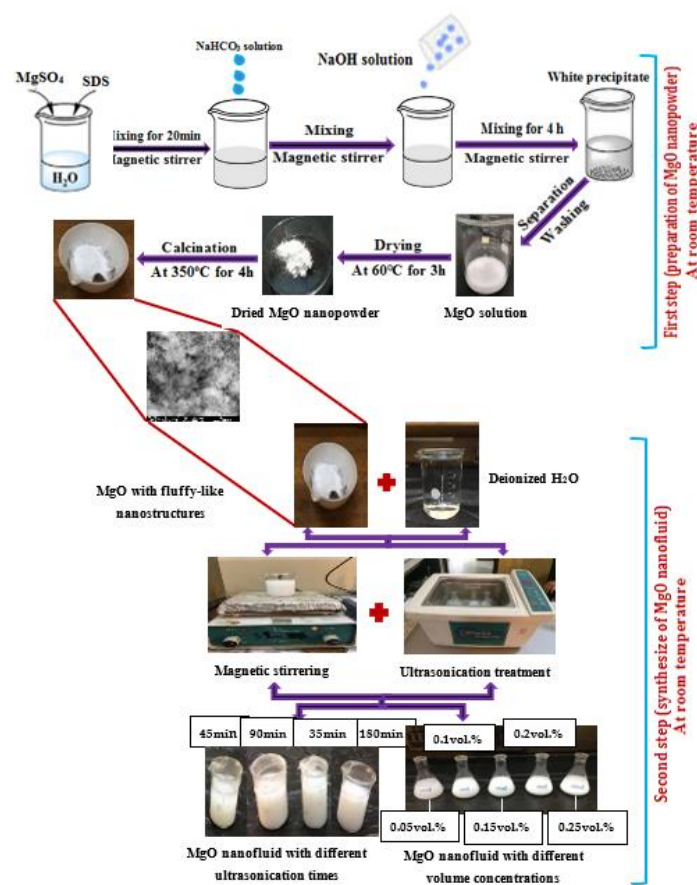


Figure 1. Synthesis of MgO -DW nanofluid via a two-step technique.

2.2. Preparation of MgO Nanofluid

A two-step technique was used to make the MgO nanofluid. The first step, i.e., nanopowder preparation, was completed (as described above). The second step involved synthesis of the nanofluid using mechanical procedures. The mechanical procedures were carried out using primary mechanical stirring for 30 min, and then ultrasonic agitation as shown in Figure 1 (second step). Different ultrasonication periods and volume concentrations were used to prepare the nanofluid samples. They were synthesized via dispersing MgO nanoparticles in 100 mL of deionized water as a base fluid without the use of any dispersants or heat. The ultrasonication times were 45, 90, 135, and 180 min. The following

relationship [67] was used to compute the volume concentration ratios of 0.05, 0.1, 0.15, 0.2, and 0.25 vol.%:

$$\phi = \frac{V_P}{V_T} \quad (1)$$

where ϕ is the volume concentration of MgO nanofluid, V_P is the volume of MgO nanopowder, and V_T is the total volume of nanofluid sample.

Depending on nanopowder density (ρ_P) and base fluid density (ρ_{bf}), the volume was measured as follows:

$$\text{Since, } V_P = \frac{m_P}{\rho_P}, \quad V_T = V_P + V_{bf} = \frac{m_P}{\rho_P} + \frac{m_{bf}}{\rho_{bf}}$$

$$\text{So, } \phi = \frac{(m_P/\rho_P)}{(m_P/\rho_P) + (m_{bf}/\rho_{bf})} \quad (2)$$

where m_P and m_{bf} are the masses of MgO nanopowder and base fluid (deionized water), respectively; ρ_P and ρ_{bf} are the densities of nanopowder and base fluid, respectively. According to the final relation, the weights of MgO nanopowder required to prepare nanofluid samples with different volume ratios are listed in Table 1.

Table 1. Weights of MgO nanoparticles corresponding to the volume concentrations.

Volume Concentrations Ratio	Weights of MgO Nanopowder (g)
0.05 vol. %	0.1433
0.1 vol. %	0.2867
0.15 vol. %	0.4326
0.2 vol. %	0.5772
0.25 vol. %	0.7178

2.3. The Characterization Techniques

The structural characteristics of MgO nanopowder were achieved using an XRD-6000 Shimadzu X-ray diffractometer with Cu K α radiation ($\lambda = 1.5406 \text{ \AA}$) in the 2θ range of $(10\text{--}80^\circ)$ in a step of 0.05° and a scan speed of 5 degree/min. A scanning electron microscope (SEM) analysis was also performed to test the surface morphology of the prepared nanopowder. The SEM device was a Mira 3-scan (Metrohm France, Villebon-sur-Yvette, France) type that ran at a 15 kV accelerating voltage. An EDX approach equipped with a SEM instrument was used to assess the composition and purity of the nanopowder.

2.4. The Stability and Particle Size Analysis

Zeta potential was employed as an index of the surface charge of the MgO nanoparticles in the base fluid. The surface charge was considered to be an indicator of the dispersion stability of the MgO nanosuspension. The suspension with high zeta potential was stabilized, while the sample with low value tended to accumulate and suffer from sedimentation, according to ASTM standard (D4187-82) of zeta potential ranges in Table 2 [68,69]. MgO-DW nanofluid samples at different concentration ratios (0.05 vol.%, 0.1 vol.%, 0.15 vol.%, 0.2 vol.%, and 0.25 vol.%) were mixed with the KCl solution, then, mechanically stirred for 30 min with ultrasonic agitation for 90 min, and then tested by the device. The same procedure was followed in the case of 0.15 vol.% MgO-DW nanofluid samples at different ultrasonication times (45, 90, 135, and 180 min).

Table 2. The ASTM standard of zeta potential ranges.

Zeta Potential Range (mV)	Stability Behavior
< ± 5	Rapid coagulation or flocculation
± 10 to ± 30	Incipient instability
± 30 to ± 40	Moderate stability
± 40 to ± 60	Good stability
> ± 61	Excellent stability

The measurements were carried out using a zeta potential analyzer (Zeta Plus (21521), power 100–240 V 50/60 Hz, USA). To ensure data reliability, each experiment was repeated three times before the mean results were estimated. After four days of preparation, the zeta potential measurements were obtained. A particle size analyzer (Zetasizer, Brookhaven Instruments, New York, NY, USA) can also detect particle size by using a dynamic light scattering (DLS) process. The container is illuminated by a laser, and the particles scatter the light which is measured using a detector. A fundamental property of Brownian motion is that small particles move much faster than large particles. There is an association between the size of a particle and its velocity due to Brownian motion. Based on this physical feature, a particle size analyzer measures the Brownian motion of the particles in a specimen and connects this to a size based on established theories [70]. Therefore, a particle size analyzer was used to determine the average particle size of the prepared MgO nanopowder at room temperature. The scattering angle and polydispersity index were 15° and 0.061, respectively.

2.5. Measurements of Thermophysical Properties

With varying volume concentrations of 0.05, 0.1, 0.15, 0.2, and 0.25 vol. percent, the thermal conductivity and dynamic viscosity of MgO-DW nanofluid were measured. They were also measured with various ultrasonication treatment times of 45, 90, 135, and 180 min. The thermal conductivity was tested using a Sweden company device (Hot Disk TPS 500 S, KIJTALEY, Johanneberg Science Park, Göteborg, Sweden), which is a type of thermal constants analyzer that uses the standard isotropic method. The dynamic viscosity measurements were carried out using a viscometer, Model HTD13145 Six-Speed Rotational Viscometer (Qingdao Haitongda Special Instrument Co., Ltd., Qingdao, China). The thermal conductivity and dynamic viscosity measurements were both achieved at room temperature. The enhancement ratio of thermal conductivity values of MgO-DW nanofluid can be estimated using the following relationship [71]:

$$\text{TCE}\% = \frac{K_{\text{nf}} - K_{\text{bf}}}{K_{\text{bf}}} * 100 \quad (3)$$

where K_{nf} and K_{bf} are the thermal conductivity of the nanofluid and the base fluid, respectively.

3. Results and Discussion

3.1. The Structural Studies

Figure 2 shows the XRD spectrum used to analyze the crystalline structure of the obtained MgO nanopowder. The pattern shows an ordered polycrystalline structure with five intense peaks. The low intensity of the diffraction background was clearly indicative of the pure phase of the intended material. Therefore, no distinguishing peaks of any impurities were discovered. The surfactant SDS [$\text{CH}_3(\text{CH}_2)_{11}\text{OSO}_3\text{Na}$] acts as a catalyst, preventing any fast reactions in the solution. In addition, it acts as a dispersion factor of the formed particles [72].

Hence, the synthesized material is of high purity, free of any secondary products, and nanoscale. The diffraction peaks at 2θ values of 36.9271°, 42.8937°, 62.2626°, 74.6169°, and 78.5795° correspond to the crystalline planes of (111), (200), (220), (311), and (222), respectively. A strong preferential orientation was observed at a diffraction angle of 42.8937° with Miller indices (200). Similar results have been reported in the literature [73,74]. The specified X-ray peaks matched well with the crystallographic structure according to the JCPDS standard file no. 45-0946 of polycrystalline MgO. The crystallite size (D) was calculated based on the full width at half maximum (FWHM) of the intensive diffraction peak (i.e., the plane 200) by using the Debye–Scherrer’s formula [75,76]:

$$D = \frac{A\lambda}{(\text{FWHM})\cos\theta} \quad (4)$$

where A is an empirical shape factor equal to 0.94, λ is the wavelength of the X-ray source, and θ is the angular position of the diffraction peak.

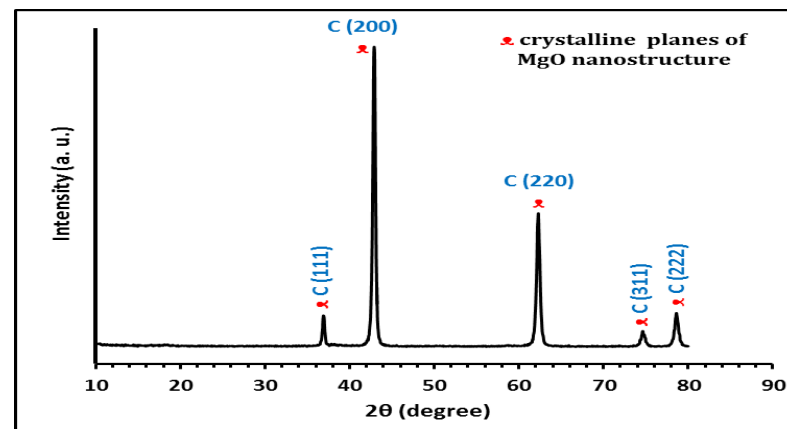


Figure 2. XRD pattern of MgO nanopowder prepared by the co-precipitation method.

The crystallite size was calculated to be 22.78 nm. The sharp diffraction peaks indicated a high degree of crystallization. The nanostructure of the prepared MgO particles was also revealed by the average particle size of less than 100 nm. All the diffraction peaks of MgO nanopowder revealed an obvious shift towards lower 2θ positions, as seen in Table 3. This result may be attributed to the nano scale of the prepared particles, whereas the high density of crystalline boundaries in the nano structure may cause microstrain.

Table 3. Positions of X-ray diffraction peaks (2θ) of MgO nanopowder prepared by the co-precipitation.

Crystalline Planes (hkl)	C (111)	C (200)	C (220)	C (311)	C (222)
Measured (XRD) 2θ (deg.)	36.9271	42.8937	62.2626	74.6169	78.5795
Standard 2θ (deg.) (JCPD S card no. 45-0946)	36.9360	42.9160	62.3020	74.6890	78.6280

The lattice constant and the unit cell volume were estimated by using the Formulas (5) and (6) [75], respectively:

$$\frac{1}{d_{(hkl)}^2} = \frac{h^2 + k^2 + l^2}{a^2} \quad (5)$$

$$V = a^3 \quad (6)$$

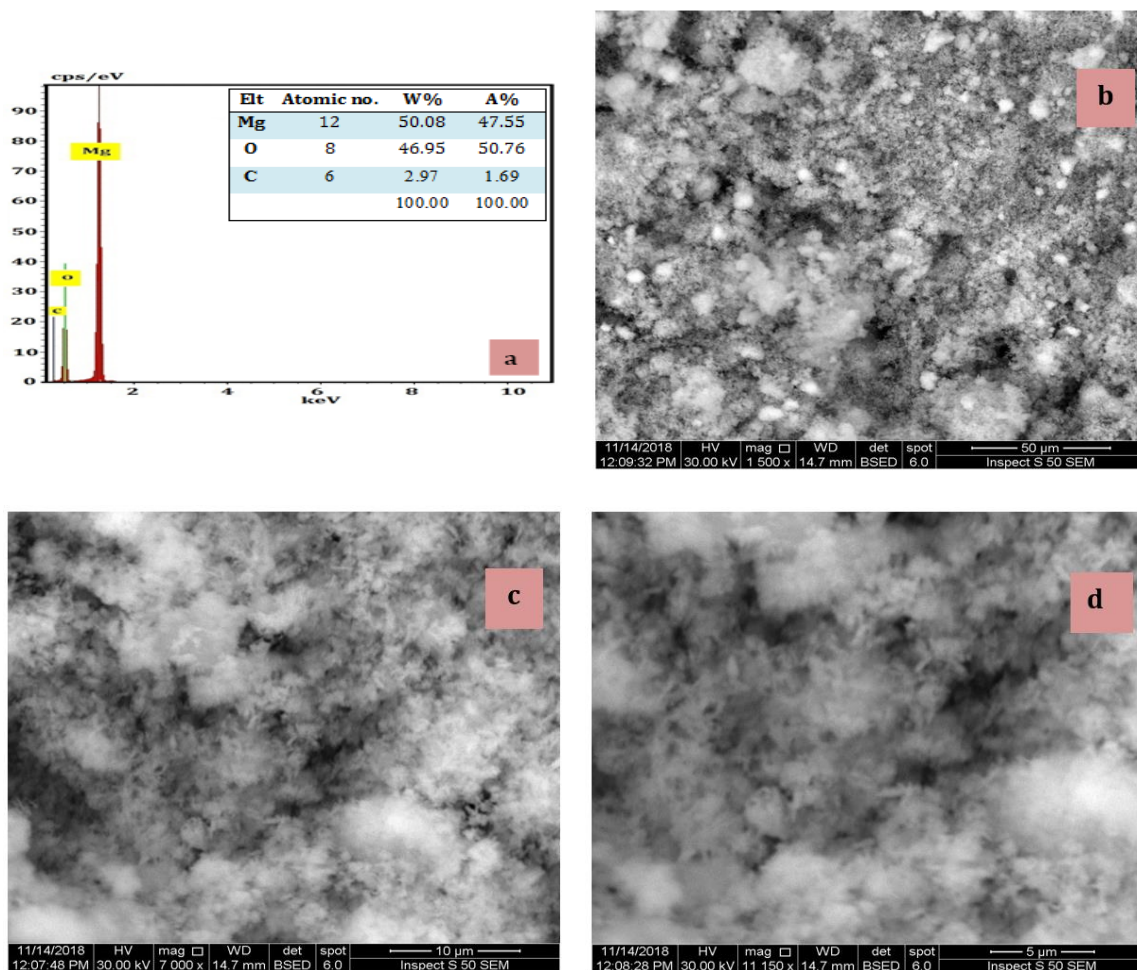
where d_{hkl} is the interplanetary crystalline distance; h , k , and l are the Miller indices; and “ a ” is the lattice constant.

From the results in Table 4, it can be noticed there is relative stretching in the d_{hkl} spacing and lattice constant values as compared with the standard values, since the variation in both is approximately 0.0011 Å of the interplanetary distance and 0.0023 Å of lattice constant. Consequently, the volume of the unit cell showed relative enlargement, which might be due to the nanoscale of MgO particles.

Table 4. XRD results of MgO nanopowder prepared by the co-precipitation method at room temperature.

The Value	Crystal Structure and (hkl)	d_{hkl} -Spacing (Å)	Lattice Constant (Å)	Unit Cell Volume (Å ³)
Measured (XRD)	Cubic (200)	2.1067	4.2135	74.8047
Standard (JCPDS card no. 45-0946)	Cubic (200)	2.1056	4.2112	74.6823

The elemental structure, purity, and surface morphology of the synthesized MgO nanostructure were tested using SEM and EDX techniques. The energy dispersive X-ray spectrum was achieved at the range of 0–10 keV, as shown in Figure 3a. One can clearly observe three evident bands at nearly 0.25 keV, 0.55 keV, and 1.3 keV which correspond to the elements of C, O, and Mg, respectively. The spectrum demonstrated a distinct absorption band of magnesium element with weight and atomic ratios of 50.08% and 47.55%, respectively. As stated in the inset table inside the Figure, the oxygen element ratios are 46.95% and 50.76%. Therefore, the EDX spectroscopy results confirmed the formation of MgO, as was previously demonstrated by XRD analysis. In addition, according to XRD results the prepared material has a pure phase, but the EDX results show a small band of carbon element.

**Figure 3.** MgO nanopowder prepared by using the co-precipitation method: (a) EDX analysis. Typical SEM images at different scale bars of: (b) 50 μm; (c) 10 μm; (d) 5 μm.

The presence of carbon peak in the prepared sample was attributed to the carbon holder utilized in the imaging and/or the sodium carbonate used in the preparation process. A similar result was reported in the literature [77]. The morphology of MgO nanostructure was anatomized at various magnifications, as displayed in Figure 3b–d. Figure 3b exhibits agglomerated structures with high density. It shows what looks like snowballs or bright white cotton balls that are diffused on the surface of the agglomerated structures. Interestingly, the SEM images (Figure 3c,d) exhibit feathery or fluffy-like nanostructures that assemble together to form dense clouds.

The fluffy-like nanostructures have varied orientations, resulting in the intermingled morphology within the clouds. The average particle size of MgO nanostructures was measured to be 33 nm.

3.2. Stability Measurement of MgO-DW Nanofluid

The stability of the nano suspension contents in the base medium must be carefully monitored since it has a significant influence on the thermal characteristics. Nanoparticle aggregation may cause precipitation and blockage, hence, decreasing the thermal conductivity of the nanofluid. The zeta potential refers to the quantity of electrostatic repulsion potential presented between the charged nanoparticles and the base fluid. The zeta potential was investigated at various volume concentrations and ultrasonication times of MgO-DW nanofluid, as listed in the Table 5A,B. It can be seen that all the values of zeta potential have a negative sign, due to the adsorption of the OH⁻ ions (negative ions) on the surface of MgO nanoparticles. The states of zeta potential values were determined according to the ASTM standard in Table 2 (experimental part). The specimens in part A were conducted with an ultrasonication time of 90 min. Mostly, the zeta potential values exhibited that as the volume ratios increased from 0.05 to 0.25 vol.%, the ZP values of the synthesized MgO-DW nanofluid decreased from −41.0 to −30.3 mV. This behavior cannot be extended as a general rule, as shown in the 0.15 vol.% MgO nanofluid sample, which recorded a zeta potential value of −47.0 mV. Hence, in the case of this sample, an increase in solid volume concentration did not cause a decrease in the zeta potential value, as shown in other samples.

Table 5. Zeta potential analysis of MgO nanofluids prepared using the two-step technique.

Volume Ratios ϕ (vol.%)	A			B	
	Zeta Potential (mV)	The State	Ultrasonication Time (min)	Zeta Potential (mV)	The State
0.05	−41.0	Good stability	45	−38.9	Moderate stability
0.1	−38.2	Moderate stability	90	−45.0	Good stability
0.15	−45.0	Good stability	135	−54.7	Good stability
0.2	−35.7	Moderate stability	180	−62.1	Good stability
0.25	−30.3	Moderate stability			

Good stability was obtained when the electrostatic repulsion forces overcame the attraction forces such as Van der Waals forces between the MgO nanoparticles. For this reason, this phenomenon could prevent accumulation, therefore, no sedimentation of dispersion nanoparticles occurred within the base fluid. A low zeta potential value was found at 0.25 vol.% MgO-DW nanofluid, which indicated the presence of some clusters or aggregates. However, this sample was moderately stable. All the samples in part B were prepared with a concentration ratio of 0.15 vol.% nanoparticles. It can be seen that ultrasonication time is directly proportional to zeta potential values. Therefore, as ultrasonication time increased from 45 to 180 min, the ZP values of the synthesized MgO nanofluids also increased from −38.9 to −62.1 mV. The portion of nanoparticles that survive in a well dispersed state in nanofluid increases as the ultrasonication treatment period increases, raising the zeta potential values. The last result confirmed the possibility

of improving the dispersion stability of the nanofluids via an increasing ultrasonication agitation time. The current findings agree with those reported in [61].

3.3. Thermophysical Properties Measurements

3.3.1. Thermal Conductivity

The thermal conductivity of MgO-DW nanofluid is one of the most important operators that has a direct effect on heat transfer rate. Variations in thermal conductivity and relative thermal conductivity with respect to the nanoparticle concentration ratio ranging from 0.05 to 0.25 vol.% was studied at room temperature $27\text{ }^{\circ}\text{C} \pm 2$, as shown in Figure 4a,b. It is apparent from Figure 4 that the thermal conductivity and relative thermal conductivity increased with the solid content of dispersed MgO nanostructures.

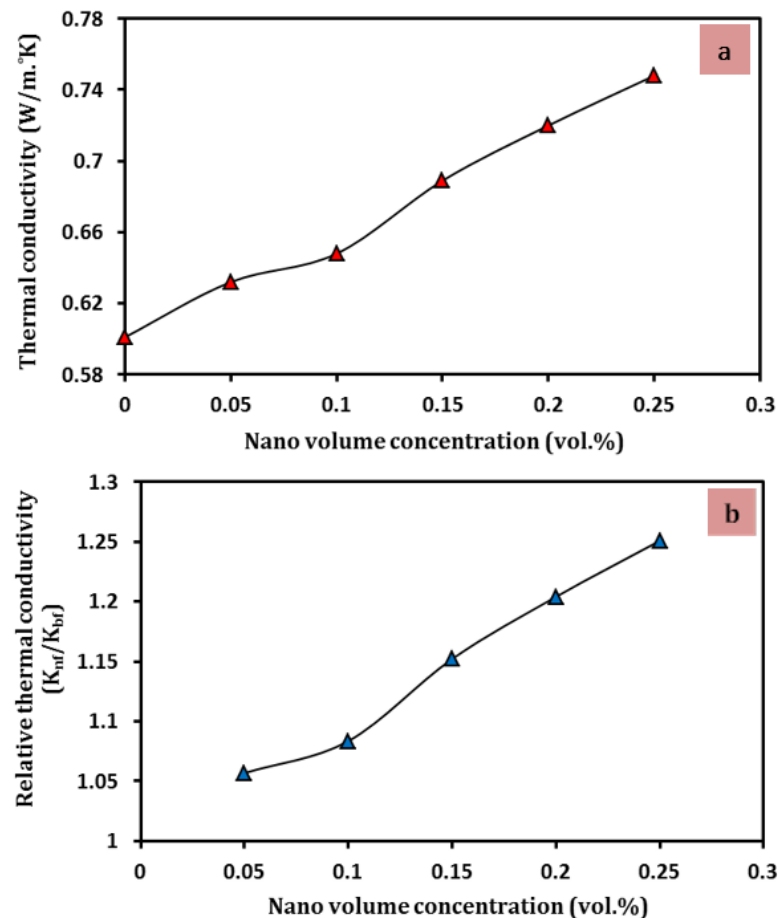


Figure 4. (a) The thermal conductivity and (b) relative thermal conductivity (K_{nf}/K_{wf}), as a function of solid volume concentration of MgO-DW nanofluid at room temperature.

The thermal conductivity of MgO is approximately $48.4\text{ (W/m}\cdot\text{K)}$ [57] which is significantly greater than water's value of $0.598\text{ (W/M}\cdot\text{K)}$ [78]. As a result, raising the concentration ratio of MgO nanopowder would undoubtedly improve and increase the thermal conductivity of the prepared nanofluid. Notably, the utilized MgO nanoparticles have a high specific surface area that comes from a nanoscale of 33 nm. Hence, there is a significant rate of heat transfer between dispersed nanoparticles and deionized water molecules, which increases as their volume concentrations increase.

In other words, an improvement in relative thermal conductivity means increased interactions between nanoparticles. The interactions are ascribed to the evolution of intense networks of dispersed nanoparticles inside the base fluid and the stir action caused by the Brownian motion of these nanoparticles. Furthermore, the Brownian motion becomes faster in the case of a nanostructure.

The greatest thermal conductivity enhancement (by using Relation (3)) was found to be 25.08% at the highest concentration of 0.25 vol.%. In addition, the lowest improvement was 5.68% at a volume concentration of 0.05 vol.%, as observed in Table 6. Generally, increasing the volume concentrations of MgO nanoparticles in the fluid minimizes the distance between moving particles, resulting in more molecular collisions. An increase in the accelerated nanoparticles in the base fluid enhances the thermal conductivity of the nanofluid.

Table 6. The improvement ratios of the thermal conductivity with solid volume concentrations of MgO/DW nanofluid at room temperature.

Concentration Ratios ϕ (vol.%)	Thermal Conductivity Enhancement (TCE%)
0.05	5.685
0.1	8.361
0.15	15.217
0.2	20.401
0.25	25.084

Furthermore, the development of clusters and aggregates can take the shape of chain-like structures which provide a transformation path of the thermal energy among the nanoparticles. This may explain the high improvement ratio of thermal conductivity in the case of 0.25 vol.% MgO-DW nanofluid, despite the low zeta potential value of this sample. The results agree very well with the researchers' observations in [79–81].

The major aim of ultrasonication treatment is to ensure proper dispersion and break up of any residual agglomerations in the dispersed phase (MgO nanopowder) within the base fluid. Figure 5 reveals the changes in thermal conductivity with respect to the ultrasonication treatment time of MgO-DW nanofluid. The evident trend in Figure 5 is that the values of thermal conductivity increase with ultrasonication time.

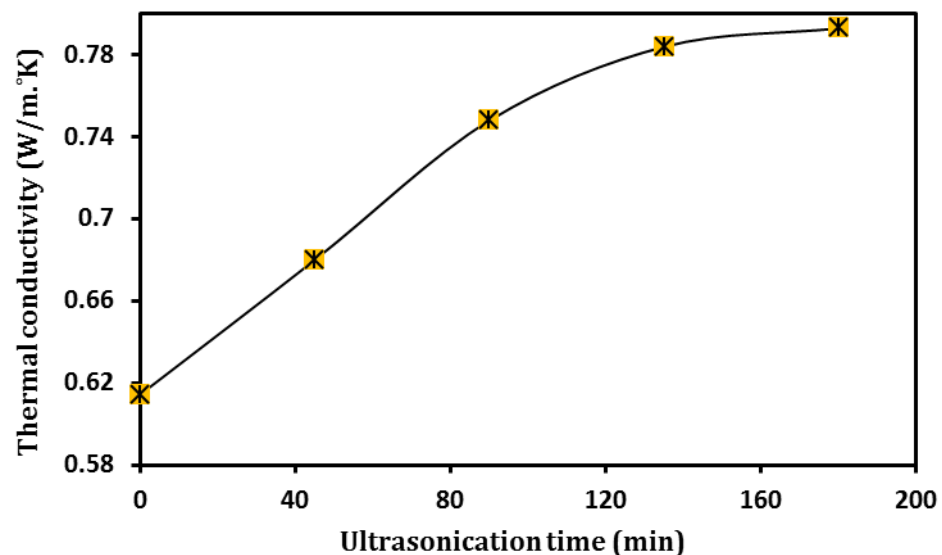


Figure 5. The thermal conductivity as a function of ultrasonication time of 0.25 vol.% MgO-DW nanofluid at room temperature.

The increase in thermal conductivity with an increase in ultrasonication time may be attributed to enhancing dispersion stability, which was confirmed via zeta potential analysis (see Table 5). Therefore, the majority of the nanoparticles in the MgO nanosuspension will participate in the heat transfer process, increasing with ultrasonication agitation time, thereby, increasing its thermal conductivity. The differences in thermal conductivity

were constrictive between 135 and 180 min of ultrasonication, and hence, ultrasonication influence was marginalized after 135 min. Therefore, the enhancement rate in thermal conductivity was insignificant over these periods, as shown in Table 7. The authors in [82–86] found a similar behavior when they investigated the thermal conductivity of MWCNT, Fe₃O₄/CNT, TiO₂, CNT, and Al₂O₃ nanofluids, respectively, at various ultrasonication times. Therefore, at the ultrasonication time of 180 min, the 0.25 vol.% MgO-DW nanofluid showed better thermal transport characteristics due to the higher volume concentration of MgO nanoparticles in the suspended state.

Table 7. The improvement ratios of the thermal conductivity with ultrasonication time of MgO-DW nanofluid at room temperature.

Concentration Ratios ϕ (vol.%)	Improvement of Thermal Conductivity (K_{nf} %)
45	13.71
90	25.08
135	31.10
180	32.61

3.3.2. Dynamic Viscosity

The concentration ratio of nanoparticles and ultrasonication time are major factors that influence the viscosity of nanofluids. Figure 6a,b shows the changes in viscosity and relative viscosity with volume concentration ratios of MgO-DW nanofluid, at room temperature.

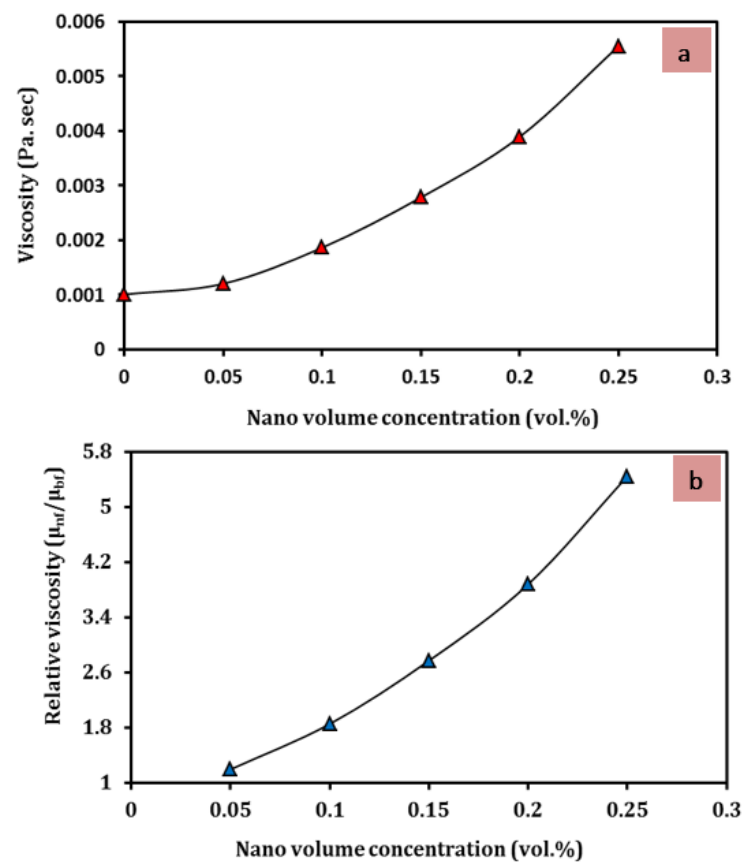


Figure 6. (a) The viscosity; (b) the relative viscosity (μ_{nf}/μ_{bf}), as a function of solid volume concentration of MgO-DW nanofluid at room temperature.

Figure 6a shows that the viscosity of MgO-DW nanofluid is directly proportional to the MgO nanoparticles loading. The viscosity of nanofluid samples was gradually increased

with increasing concentrations of MgO nanopowder. The intersection on the viscosity axis corresponded to the viscosity value of base fluid as 0.001 (Pa·sec). The increase in nanofluid viscosity is narrow over the range of nanoparticle concentration of ≤ 0.05 vol.%, while the increasing is fast over a range of more than 0.05 to 0.25 vol.% of the MgO nanoparticle concentration. Furthermore, the resistance to flow increased to 0.0052 (Pa·Sec) at a higher solid content of 0.25 vol.% MgO-DW nanofluid. The dynamic viscosity behavior of MgO-DW nanofluid is harmonious with the predictions in [87,88]. The viscosity of nanofluids is compared to that of base fluid producing relative viscosity, as seen in Figure 6b. It shows how much the nanofluid viscosity differs from the viscosity of the base fluid. From Figure 6, it can be observed that the relative viscosity increases with increasing volume concentrations of MgO-DW nanofluid.

The lowest value of relative viscosity, i.e., 1.2, was obtained by 0.05 vol.% MgO-DW nanofluid, with respect to a base fluid viscosity, while the higher value was obtained by nano solid content of 0.25 vol.%. When the MgO nanoparticle content increases within the base fluid, the Brownian motion is restricted as a result of intense collisions between nanoparticles. Subsequently, the relative viscosity of MgO-DW nanofluid increases with nanopowder volume concentration.

The effects of ultrasonication time on the viscosity of the MgO-DW nanofluid were investigated, as shown in Figure 7. The results show that the viscosity experiences a sharp decrease by increasing the ultrasonication treatment time.

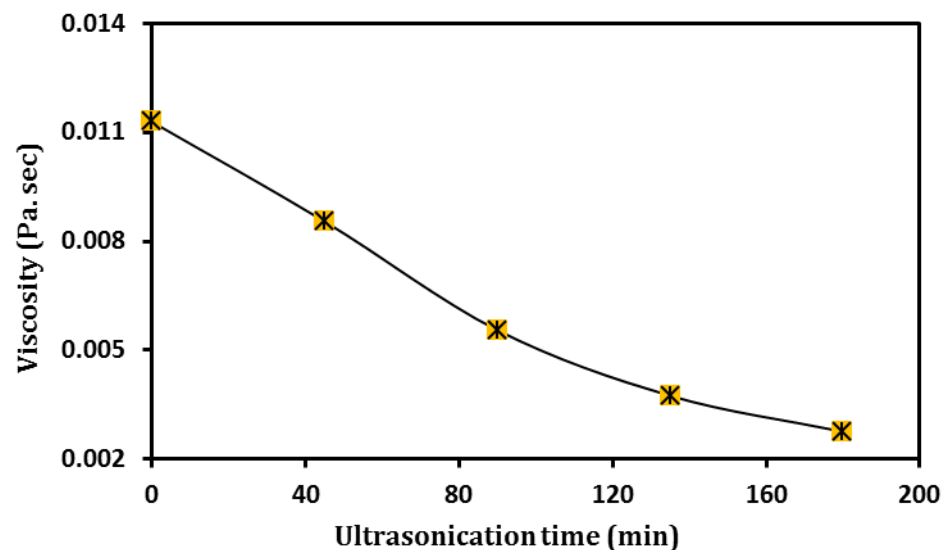


Figure 7. The viscosity as a function of ultrasonication time of 0.25 vol.% MgO-DW nanofluid at room temperature.

On the one hand, the minimal value of dynamic viscosity was measured at 180 min of ultrasonication treatment, indicating a decreasing tendency. On the other hand, the maximum value of viscosity was obtained by the nanofluid sample which was synthesized by stirring only without ultrasonication treatment of 0.0122 Pa·sec. This trend is identical to the results reported by A. Asadi et al. [89] and I. M. Mahbulul et al. [90]. Because the nanoparticles are uniformly dispersed in the base fluid, there are few or no clusters. As a result, the majority of nanoparticles, if not all, are involved in the flow, lowering the resistance to the viscometer's spindle. Additionally, the motion of the various layers of the nanofluid is made easier, hence, the dynamic viscosity decreases.

It is worth noting that increasing the ultrasonication time improves the dispersion stability and the thermal conductivity, while decreasing the dynamic viscosity of the prepared nanofluid. Ultrasonication time and dynamic viscosity are highly important in engineering applications where both of them have direct influences on the heat transfer performance, pumping power, and pressure drop.

4. Conclusions

A novel two-step technique was employed for preparing efficient MgO-DW nanofluid, at room temperature, without using surfactants and/or organic base fluids. Based on the experimental valuation, the following conclusions can be drawn:

- The co-precipitation method was followed to make crystalline and pure MgO nanopowder with an average particle size of 33 nm.
- SEM images revealed unique feathery or fluffy-like nanostructures of the prepared MgO nanopowder.
- MgO-DW nanofluid was synthesized with volume concentrations ranging from 0.05 to 0.25 vol.%, and ultrasonication treatment times ranging from 45 to 180 min, at room temperature.
- Zeta potential results showed that good stability was obtained with nano MgO content of 0.15 vol.% and a higher ultrasonication time of 180 min.
- The addition of MgO nanoparticles to traditional fluid as DW improved its thermal conductivity, where the highest value of thermal conductivity enhancement of 25.08% was found at 0.25 vol.% concentration and 180 min ultrasonication time.
- The effect of ultrasonication time on thermal conductivity improvement was similar to the impact of the nanoparticles volume concentration. However, this enhancement in the conductivity became limited after an ultrasonication time of 135 min.
- The dynamic viscosity measurements were revealed as directly proportional to the volume concentration of MgO-DW nanofluids, until recording the highest value of 0.0052 (Pa·Sec) at a higher solid content of 0.25 vol.% MgO-DW nanofluid. On the contrary, an increase in ultrasonication time resulted in a sharp decrease in the viscosity of the nanofluid samples.
- An MgO-DW nanofluid with good dispersion stability, high thermal conductivity, and low viscosity was created by controlling ultrasonication time and/or volume concentration.
- The produced MgO-DW nanofluid has the potential for exploitation in various implementations such as working fluid in cooling systems and heat exchangers. Therefore, it can be used as a working fluid in a hybrid solar collector, to study the effect of different flow rates on electrical and thermal efficiency.

Author Contributions: Methodology, H.K.J., A.G.T.A.-H. and F.N.A.Z.; investigation, H.K.J., A.G.T.A.-H., F.N.A.Z. and W.A.K.A.-M.; writing—original draft preparation, H.K.J., A.G.T.A.-H. and F.N.A.Z.; writing—review and editing, H.K.J., W.A.K.A.-M. and F.A.; supervision, B.E. All authors have read and agreed to the published version of the manuscript.

Funding: This research received no external funding.

Acknowledgments: We acknowledge support by the Deutsche Forschungsgemeinschaft (DFG) German Research Foundation and the Open Access Publishing Fund of the Technical University of Darmstadt. The authors would like to also thank the University of Technology-Iraq.

Conflicts of Interest: The authors declare no conflict of interest.

Nomenclature

MgO	Magnesium oxide
DW	Deionized water
SSA	Specific surface area
CuO	Copper oxide
Al ₂ O ₃	Aluminum oxide
ZnO	Zinc oxide
TiO ₂	Titanium oxide
Fe ₂ O ₃	Iron oxide
EG	Ethylene glycol

LiNO ₃	Lithium nitrate
NaNO ₃	Sodium nitrate
KNO ₃	Potassium nitrate
CTAB	Cetyl trimethylammonium bromide
ϕ	Volume concentration ratio
V _P	Volume of nanopowder
V _T	Total volume of nanofluid
ρ_P	Nanopowder density
ρ_{bf}	Base fluid density
m _P	Mass of nanopowder
m _{bf}	Mass of base fluid
TCE	Thermal conductivity enhancement
K _{nf}	Thermal conductivity of nanofluid
K _{bf}	Thermal conductivity of base fluid
JCPDS	Joint committee of powder diffraction standards
D	Crystallite size
V	Volume of unit cell
θ	Diffraction Angle of X-ray
d _{hkl}	Interplaner crystalline distance
hkl	Miller indices
a	Lattice constant
FWHM	Full width at half maximum of the X-ray diffraction peak.
ZP	Zeta potential
MWCT	Multi-walled carbon nanotubes
vol.%	Volume percentage
μ_{nf}	Viscosity of nanofluid
μ_{bf}	Viscosity of base fluid

References

1. Hashim, A.A. (Ed.) *Smart Nanoparticles Technology*; IntechOpen: Rijeka, Croatia, 2012.
2. Das, S.K.; Choi, S.U.; Yu, W.; Pradeep, T. *Nanofluids, Science and Technology*; John Wiley & Sons Inc.: Hoboken, NJ, USA, 2008.
3. Waqas, H.; Farooq, U.; Muhammad, T.; Manzoor, U. Importance of shape factor in Sisko nanofluid flow considering gold nanoparticles. *Alex. Eng. J.* **2022**, *61*, 3665–3672. [[CrossRef](#)]
4. Bharat, B.; Baral, D. *Nanofluids for Heat and Mass Transfer (Fundamentals, Sustainable Manufacturing and Applications)*, 1st ed.; Elsevier: Amsterdam, The Netherlands, 2021.
5. Esfe, M.H.; Arani, A.A.A.; Rezaie, M.; Yan, W.-M.; Karimipour, A. Experimental determination of thermal conductivity and dynamic viscosity of Ag–MgO/water hybrid nanofluid. *Int. Commun. Heat Mass Transf.* **2015**, *66*, 189–195. [[CrossRef](#)]
6. Gonçalves, I.; Souza, R.; Coutinho, G.; Miranda, J.; Moita, A.; Pereira, J.E.; Moreira, A.; Lima, R. Thermal Conductivity of Nanofluids: A Review on Prediction Models, Controversies and Challenges. *Appl. Sci.* **2021**, *11*, 2525. [[CrossRef](#)]
7. Ali, N.; Teixeira, J.A.; Addali, A. A Review on Nanofluids: Fabrication, Stability, and Thermophysical Properties. *J. Nanomater.* **2018**, *2018*, 6978130. [[CrossRef](#)]
8. Ali, N.; Bahman, A.M.; Aljuwayhel, N.F.; Ebrahim, S.A.; Mukherjee, S.; Alsayegh, A. Carbon-Based Nanofluids and Their Advances towards Heat Transfer Applications—A Review. *Nanomaterials* **2021**, *11*, 1628. [[CrossRef](#)] [[PubMed](#)]
9. Chamsa-ard, W.; Brundavanam, S.; Fung, C.C.; Fawcett, D.; Poinern, G. Nanofluid Types, Their Synthesis, Properties and Incorporation in Direct Solar Thermal Collectors: A Review. *Nanomaterials* **2017**, *7*, 131. [[CrossRef](#)]
10. Maxwell, J.C. *Electricity and Magnetism*; Clarendon Press: Oxford, UK, 1873.
11. Maxwell, J.C. *A Treatise on Electricity and Magnetism*; Clarendon Press: Oxford, UK, 2010; Volume 1.
12. Choi, S.U.S. *Enhancing Thermal Conductivity of Fluids with Nanoparticles*; ASME: New York, NY, USA, 1995; Volume 66, pp. 99–105.
13. Judran, H.K. Preparation and Investigation Study on (CuO/H₂O) Nanofluid for Improving the Performance of (PV/T) Hybrid System. Ph.D. Thesis, University of Technology, Baghdad, Iraq, 2016.
14. Koblinski, P.; Eastman, J.A.; Cahill, D.G. Nanofluids for thermal transport (review). *Annu. Rev. Mater. Res.* **2005**, *8*, 36–44.
15. Terekhov, V.I.; Kalinina, S.V.; Lemanov, V.V. The mechanism of heat transfer in nanofluids: State of the art (review). Part1. Synthesis and properties of nanofluids. *Thermophys. Aeromechanics* **2010**, *17*, 1–14. [[CrossRef](#)]
16. Tarafdar, A.; Negi, T.; Badgujar, P.C.; Shahi, N.C.; Kumar, S.; Sim, S.; Pandey, A. Nanofluid research advances: Preparation, characteristics and applications in food processing. *Food Res. Int.* **2021**, *150*, 110751. [[CrossRef](#)]
17. Babar, H.; Ali, H.M. Towards hybrid nanofluids: Preparation, thermophysical properties, applications and challenges. *J. Mol. Liq.* **2019**, *281*, 598–633. [[CrossRef](#)]
18. Esfe, M.H.; Saedodin, S.; Asadi, A.; Karimipour, A.; Ali, H.M. Thermal conductivity and viscosity of Mg(OH)₂-ethylene glycol nanofluids. Finding a critical temperature. *J. Therm. Anal. Calorim.* **2015**, *120*, 1145–1149. [[CrossRef](#)]

19. Safaei, M.R.; Hajizadeh, A.; Afrand, M.; Qi, C.; Yarmand, H.; Zulkifli, N.W.B. Evaluating the effect of temperature and concentration on the thermal conductivity of ZnO-TiO₂/EG hybrid nanofluid using artificial neural network and curve fitting on experimental data. *Phys. A Stat. Mech. Appl.* **2019**, *519*, 209–216. [[CrossRef](#)]
20. Asadi, A.; Pourfattah, F. Heat transfer performance of two oil-based nanofluids containing ZnO and MgO nanoparticles; a comparative experimental investigation. *Powder Technol.* **2019**, *343*, 296–308. [[CrossRef](#)]
21. Shahsavari, A.; Khanmohammadi, S.; Karimipour, A.; Goodarzi, M. A novel comprehensive experimental study concerned synthesizes and prepare liquid paraffin-Fe₃O₄ mixture to develop models for both thermal conductivity & viscosity: A new approach of GMDH type of neural network. *Int. J. Heat Mass Transf.* **2019**, *131*, 432–441.
22. Goodarzi, M.; Toghraie, D.; Reiszadeh, M.; Afrand, M. Experimental evaluation of dynamic viscosity of ZnO-MWCNTs/engine oil hybrid nanolubricant based on changes in temperature and concentration. *J. Therm. Anal. Calorim.* **2019**, *136*, 513–525. [[CrossRef](#)]
23. Bioucas, F.E.B.; Rausch, M.H.; Schmidt, J.; Bück, A.; Kolle, T.M.; Fröba, A.P. Effective Thermal Conductivity of Nanofluids: Measurement and Prediction. *Int. J. Thermophys.* **2020**, *41*, 55. [[CrossRef](#)]
24. Mahbubul, I.M. *Preparation, Characterization, Properties, and Application of Nanofluid*, 1st ed.; William Andrew: Norwich, NY, USA, 2018.
25. Pourpasha, H.; Farshad, P.; Heris, S.Z. Modeling and optimization the effective parameters of nanofluid heat transfer performance using artificial neural network and genetic algorithm method. *Energy Rep.* **2021**, *7*, 8447–8464. [[CrossRef](#)]
26. Puneeth, V.; Baby, A.K.; Manjunatha, S. The analogy of nanoparticle shapes on the theory of convective heat transfer of Au-Fe₃O₄ Casson hybrid nanofluid. *Heat Transf.* **2021**, *3*, 1–18.
27. Junankar, A.A.; Parate, S.R.; Dethé, P.K.; Dhote, N.R.; Gadkar, D.G.; Gadkar, D.D.; Gajbhiye, S.A. A Review: Enhancement of turning process performance by effective utilization of hybrid nanofluid and MQL. *Mater. Today Proc.* **2021**, *38*, 44–47. [[CrossRef](#)]
28. Jawad, M.; Saeed, A.; Gul, T.; Shah, Z.; Kumam, P. Unsteady thermal Maxwell power law nanofluid flow subject to forced thermal Marangoni Convection. *Sci. Rep.* **2021**, *11*, 7521.
29. Waqas, H.; Manzoor, U.; Shah, Z.; Arif, M.; Shutaywi, M. Magneto-Burgers Nanofluid Stratified Flow with Swimming Motile Microorganisms and Dual Variables Conductivity Configured by a Stretching Cylinder/Plate. *Math. Probl. Eng.* **2021**, *2021*, 8817435. [[CrossRef](#)]
30. Acharya, N.; Mabood, F.; Shahzad, S.A.; Badruddin, I.A. Hydrothermal variations of radiative nanofluid flow by the influence of nanoparticles diameter and nanolayer. *Int. Commun. Heat Mass Transf.* **2022**, *130*, 105781. [[CrossRef](#)]
31. Suganthi, K.S.; Rajan, K.S. Metal oxide nanofluids: Review of formulation, thermo-physical properties, mechanisms, and heat transfer performance. *Renew. Sustain. Energy Rev.* **2017**, *76*, 226–255. [[CrossRef](#)]
32. Porgar, S.; Rahmanian, N. *Investigation of Effect of Aluminium Oxide Nanoparticles on the Thermal Properties of Water-Based Fluids in a Double Tube Heat Exchanger*; University of Bradford: Bradford, UK, 2022; Volume 12, pp. 2618–2628.
33. Dahkaee, K.P.; Sadeghi, M.T.; Khroueian, Z.F.; Esmailzadeh, P. Effect of NiO/SiO₂ nanofluids on the ultra-interfacial tension reduction between heavy oil and aqueous solution and their use for wettability alteration of carbonate rocks. *J. Pet. Sci. Eng.* **2019**, *176*, 11–26. [[CrossRef](#)]
34. Yang, L.; Hu, Y. Toward TiO₂ Nanofluids Part1: Preparation and Properties. *Nanoscale Res. Lett.* **2017**, *12*, 417.
35. Maseer, M.M.; Alnaimi, F.B.I.; Hannun, R.M.; Al-Gburi, K.A.H.; Mezan, S.O. A review of the characters of nanofluids used in the cooling of a photovoltaic thermal collector. *Mater. Today Proc.* **2021**, 1–9. [[CrossRef](#)]
36. Sone, B.T.; Diallo, A.; Fukui, X.G.; Gurib-Fakim, A.; Maaza, M. Biosynthesized CuO nano-platelets: Physical properties and enhanced thermal conductivity nanofluidics. *Arab. J. Chem.* **2018**, *13*, 160–170. [[CrossRef](#)]
37. Abbas, F.; Ali, H.M.; Shaban, M.; Janjua, M.M.; Doranehgard, M.H.; Ahmadlouydarab, M.; Farukh, F. Towards convective heat transfer optimization in aluminum tube automotive radiators: Potential assessment of novel Fe₂O₃-TiO₂/water hybrid nanofluid. *J. Taiwan Inst. Chem. Eng.* **2021**, *14*, 424–436. [[CrossRef](#)]
38. Lai, Y.F.; Chaudouët, P.; Charlot, F.; Matko, I.; Dubourdieu, C. Magnesium oxide nanowires synthesized by pulsed liquid-injection metal organic chemical vapor deposition. *Appl. Phys. Lett.* **2009**, *94*, 022904. [[CrossRef](#)]
39. Hornak, J. Synthesis, Properties, and Selected Technical Applications of Magnesium Oxide Nanoparticles: A Review. *Int. J. Mol. Sci.* **2021**, *22*, 12752. [[CrossRef](#)]
40. Rane; Kanny, A.V.; Abitha, K.; Thomas, V.K. Chapter 5-Methods for Synthesis of Nanoparticles and Fabrication of Nanocomposites. In *Synthesis of Inorganic Nanomaterials*; Micro and Nano Technologies; Wood Head Publishing: Cambridge, UK, 2018; pp. 121–139.
41. Mehta, M.; Mukhopadhyay, M.; Christian, R.; Mistry, N. Synthesis and characterization of MgO nanocrystals using strong and weak bases. *Powder Technol.* **2012**, *226*, 213–221. [[CrossRef](#)]
42. Thamilvanan, D.; Jeevanandam, J.; Hii, Y.S.; Chan, Y.S. Sol-gel coupled ultrasound synthesis of photo-activated magnesium oxide nanoparticles: Optimization and antibacterial studies. *Can. J. Chem. Eng.* **2021**, *99*, 502–518. [[CrossRef](#)]
43. Niu, F.; Meier, A.L.; Wessels, B.W. Epitaxial growth and strain relaxation of MgO thin films on Si grown by molecular beam epitaxy. *J. Vac. Sci. Technol. B* **2006**, *24*, 2586–2591. [[CrossRef](#)]
44. Pradita, T.; Shih, S.J.; Aji, B.B.; Sudiby. Synthesis of MgO powder from magnesium nitrate using spray pyrolysis. In *International Conference on Chemistry*; Chemical Process and Engineering (IC3PE), AIP Conf. Proc. 1823, (020016-1)-(020016-5); AIP Publishing: New York, NY, USA, 2017.

45. Alavi, M.A.; Morsali, A. Syntheses and characterization of Mg(OH)₂ and MgO nanostructures by ultrasonic method. *Ultrason. Sonochem.* **2010**, *17*, 441–446. [[CrossRef](#)] [[PubMed](#)]
46. Gajengi, A.L.; Sasaki, T.; Bhanage, B.M. Mechanistic aspects of formation of MgO nanoparticles under microwave irradiation and its catalytic application. *Adv. Powder Technol.* **2017**, *28*, 1185–1192. [[CrossRef](#)]
47. Sirota, V.; Selemenev, V.; Kovaleva, M.; Pavlenko, I.; Mamunin, K.; Dokalov, V.; Prozorova, M. Synthesis of Magnesium Oxide Nanopowder by Thermal Plasma Using Magnesium Nitrate Hexahydr. *Phys. Res. Int.* **2016**, *2016*, 6853405. [[CrossRef](#)]
48. Ouraipryvan, P.; Sreethawong, T.; Chavadej, S. Synthesis of crystalline MgO nanoparticle with mesoporous-assembled structure via a surfactant-modified sol-gel process. *Mater. Lett.* **2009**, *63*, 1862–1865. [[CrossRef](#)]
49. Stojanovic, B.D.; Dzunuzovic, A.S.; Ilic, N.I. 17-Review of methods for the preparation of magnetic metal oxides. In *Magnetic, Ferroelectric, and Multiferroic Metal Oxides (Metal Oxides)*; Elsevier: Amsterdam, The Netherlands, 2018; pp. 333–359.
50. Feng, S.-H.; Li, G.-H. Hydrothermal and Solvothermal Syntheses. In *Modern Inorganic Synthetic Chemistry*, 2nd ed.; Xu, R., Xu, Y., Eds.; Elsevier: Amsterdam, The Netherlands, 2017; pp. 73–104.
51. Yang, Q.; Sha, J.; Wang, L.; Wang, J.; Yang, D. MgO nanostructures synthesized by thermal evaporation. *Mater. Sci. Eng. C* **2006**, *26*, 1097–1101. [[CrossRef](#)]
52. Ngo, C.; Voorde, C.; van de Voorde, M.H. *Nanotechnology in a Nutshell: From Simple to Complex Systems*; Atlantis Press: Paris, France, 2014.
53. Saied, E.; Eid, A.M.; Hassan, S.E.D.; Salem, S.S.; Radwan, A.A.; Halawa, M.; Saleh, F.M.; Saied, E.M.; Fouda, A. The Catalytic Activity of Biosynthesized Magnesium Oxide Nanoparticles (MgO-NPs) for Inhibiting the Growth of Pathogenic Microbes, Tanning Effluent Treatment and Chromium Ion Removal. *Catalysts* **2021**, *11*, 821. [[CrossRef](#)]
54. Faisal, F.S.; AslamKhan, M.; Rizwan, M.; Hussain, Z.; Zaman, N.; Afsheen, Z.; Uddin, M.N.; Bibi, N. Exploring the therapeutic potential of Hibiscus rosa sinensis synthesized cobalt oxide (Co₃O₄-NPs) and magnesium oxide nanoparticles (MgO-NPs). *Saudi J. Biol. Sci.* **2021**, *28*, 5157–5167.
55. Pal, G.; Rai, P.; Pandey, A. Chapter 1-Green synthesis of nanoparticles: A greener approach for a cleaner future. In *Green Synthesis, Characterization and Applications of Nanoparticles (Micro and Nano Technologies)*; Elsevier: Amsterdam, The Netherlands, 2019; pp. 1–26.
56. Singh, J.P.; Singh, V.; Sharma, A.; Pandey, G.; Chae, K.H.; Lee, S. Approaches to synthesize MgO nanostructures for diverse applications. *Heliyon* **2020**, *6*, e04882. [[CrossRef](#)] [[PubMed](#)]
57. Manikandan, S.; Rajan, K.S. Rapid synthesis of MgO nanoparticles & their utilization for formulation of a propylene glycol based nanofluid with superior transport properties. *RSC Adv.* **2014**, *4*, 1830–1837.
58. Esfe, M.H.; Afrand, M.; Karimipour, A.; Yan, W.-M.; Sina, N. An experimental study on thermal conductivity of MgO nanoparticles suspended in a binary mixture of water and ethylene glycol. *Int. Commun. Heat Mass Transf.* **2015**, *67*, 173–175. [[CrossRef](#)]
59. Yapici, K.; Osturk, O.; Uludag, Y. Dependency of nanofluid rheology on particle size and concentration of various metal oxide nanoparticles. *Braz. J. Chem. Eng.* **2018**, *35*, 575–586. [[CrossRef](#)]
60. Lu, J.; Zhang, Z.; Wang, W.; Ding, J. Effects of MgO Nanoparticles on Thermo-Physical Properties of LiNO₃-NaNO₃-KNO₃ for Thermal Energy Storage. *Energies* **2021**, *14*, 677. [[CrossRef](#)]
61. Nfawa, S.R.; Talib, A.R.A.; Basri, A.A.; Masuri, S.U. Novel use of MgO nanoparticle additive for enhancing the thermal conductivity of CuO/water nanofluid. *Case Stud. Therm. Eng.* **2021**, *27*, 101279. [[CrossRef](#)]
62. Saufi, M.A.B.; Mamat, H.B. A Review on Thermophysical Properties for Heat Transfer Enhancement of Carbon-Based Nanolubricant. *Adv. Eng. Mater.* **2021**, *23*, 2100403. [[CrossRef](#)]
63. Vafaei, M.; Afrand, M.; Sina, N.; Teimouri, H. Evaluation of thermal conductivity of MgO-MWCNTs/EG hybrid nanofluids based on experimental data by selecting optimal artificial neural networks. *Phys. E Low-Dimens. Syst. Nanostruct.* **2017**, *85*, 90–96. [[CrossRef](#)]
64. Mousavi, S.M.; Esmaeilzadeh, F.; Wang, X.P. Effects of temperature and particles volume concentration on the thermophysical properties and the rheological behavior of CuO/MgO/TiO₂, aqueous ternary hybrid nanofluid: Experimental investigation. *J. Anal. Calorim.* **2019**, *137*, 879–901. [[CrossRef](#)]
65. Mousavi, S.M.; Esmaeilzadeh, F.; Wang, X.P. A detailed investigation on the thermo-physical and rheological behavior of MgO/TiO₂ aqueous dual hybrid nanofluid. *J. Mol. Liq.* **2019**, *282*, 323–339. [[CrossRef](#)]
66. Bhattad, A.; Sarkar, J.; Ghosh, P. Hydrothermal performance of different alumina hybrid nanofluid types in plate heat exchanger: Experimental study. *J. Therm. Anal. Calorim.* **2020**, *139*, 3777–3787. [[CrossRef](#)]
67. Hussein, M.A.; Sharma, K.V.; Bakar, R.A.; Kadirgama, K. The Effect of Nanofluid Volume Concentration on Heat Transfer and Friction Factor inside a Horizontal Tube. *J. Nanomater.* **2013**, *2013*, 1–12. [[CrossRef](#)]
68. Hunter, R.J. *Zeta Potential in Colloid Science, Principles and Applications*, 1st ed.; Academic Press: Cambridge, MA, USA, 1988.
69. Zainon, S.N.M.; Azmi, W.H. Recent Progress on Stability and Thermo-Physical Properties of Mono and Hybrid towards Green Nanofluids. *Micromachines* **2021**, *12*, 176. [[CrossRef](#)]
70. Washington, C. *Particle Size Analysis in Pharmaceuticals and other Industries: Theory and Practice*; Ellis Horwood Limited: Chichester, UK, 1992.
71. Bianco, V.; Manca, O.; Nardini, S.; Vafai, K. *Heat Transfer Enhancement with Nanofluids*. Routledge (Taylor & Francis Group), 1st ed.; CRC Press: Boca Raton, FL, USA, 2017.

72. Sabeeh, S.H.; Hussein, H.A.; Judran, H.K. Synthesis of a complex nanostructure of CuO via a coupled chemical route. *Mater. Res. Express* **2016**, *3*, 125025. [[CrossRef](#)]
73. Wahhab, H.A.A.; Al-Maliki, W.A.K. Application of a Solar Chimney Power Plant to Electrical Generation in Covered Agricultural Fields. In *IOP Conference Series: Materials Science and Engineering*; IOP Publishing: Kerbala, Iraq, 2020; p. 012137.
74. Ammulu, M.A.; Viswanath, K.V.; Giduturi, A.K.; Vemuri, P.K.; Mangamuri, U.; Poda, S. Phytoassisted synthesis of magnesium oxide nanoparticles from *Pterocarpus marsupium* rox.b heartwood extract and its biomedical applications. *J. Genet. Eng. Biotechnol.* **2021**, *19*, 21. [[CrossRef](#)] [[PubMed](#)]
75. Cullity, B.D. *Elements of X-ray Diffraction*, 3rd ed.; Wesley Publishing Company: Boston, MA, USA, 1967.
76. Sabeeh, S.H.; Hussein, H.A.; Judran, H.K. Effect of Cu Salt Molarity on the Nanostructure of CuO Prolate Spheroid. *Int. J. Nanosci.* **2016**, *15*, 1650034. [[CrossRef](#)]
77. Wong, C.W.; Chan, Y.S.; Jeevanandam, J.; Pal, K.; Bechelany, M.; Elkodous, M.A.; El-Sayyad, G.S. Response Surface Methodology Optimization of Mono-dispersed MgO Nanoparticles Fabricated by Ultrasonic-Assisted Sol–Gel Method for Outstanding Antimicrobial and Antibiofilm Activities. *J. Clust. Sci.* **2019**, *31*, 367–389. [[CrossRef](#)]
78. Chang, M.-H.; Liu, H.-S.; Tai, C.Y. Preparation of copper oxide nanoparticles and its application in nanofluid. *Powder Technol. J.* **2011**, *207*, 378–386. [[CrossRef](#)]
79. Al-Maliki, W.; Mahmoud, N.; Al-Khafaji, H.; Alobaid, F.; Epple, B. Design and Implementation of the Solar Field and Thermal Storage System Controllers for a Parabolic Trough Solar Power Plant. *Appl. Sci.* **2021**, *11*, 6155. [[CrossRef](#)]
80. Wang, S.; Li, Y.; Zhang, H.; Lin, Y.X.; Li, Z.; Wang, W.; Wu, Q.; Qian, Y.; Hong, H.; Zhi, C. Enhancement of thermal conductivity in water-based nanofluids employing TiO₂/reduced graphene oxide composites. *J. Mater. Sci.* **2016**, *51*, 10104–10115. [[CrossRef](#)]
81. Moradikazerouni, A.; Hajizadeh, A.; Safaei, M.R.; Afrand, M.; Yarmand, H.; Zulkifli, N.W.B.M. Assessment of thermal conductivity enhancement of nano-antifreeze containing single-walled carbon nanotubes: Optimal artificial neural network and curve-fitting. *Phys. A Stat. Mech. Appl.* **2019**, *521*, 138–145. [[CrossRef](#)]
82. Asadi, A.; Alarifi, I.M.; Ali, V.; Nguyen, H.M. An experimental investigation on the effects of ultrasonication time on stability and thermal conductivity of MWCNT-water nanofluid: Finding the optimum ultrasonication time. *Ultrason. Sonochem.* **2019**, *58*, 104639. [[CrossRef](#)] [[PubMed](#)]
83. Shahsavar, A.; Salimpour, M.R.; Saghafian, M.; Shafii, M.B. An experimental study on the effect of ultrasonication on thermal conductivity of ferrofluid loaded with carbon nanotubes. *Thermochim. Acta* **2015**, *617*, 102–110. [[CrossRef](#)]
84. Mahbulul, I.M.; Elcioglu, E.B.; Saidur, R.; Amalina, M.A. Optimization of ultrasonication period for better dispersion and stability of TiO₂-water nanofluid. *Ultrason. Sonochem.* **2017**, *37*, 360–367. [[CrossRef](#)]
85. Sadri, R.; Ahmadi, G.; Togun, H.; Dahari, M.; Kazi, S.N.; Sadeghinezhad, E.; Zubir, N. An experimental study on thermal conductivity and viscosity of nanofluids containing carbon nanotubes. *Nanoscale Res. Lett.* **2014**, *9*, 151. [[CrossRef](#)]
86. Michael, M.; Zagabathuni, A.; Sikdar, S.; Pabi, S.K.; Ghosh, S. Effect of dispersion behavior on the heat transfer characteristics of alumina nanofluid: An experimental investigation and development of a new correlation function. *Int. Nano Lett.* **2020**, *10*, 207–217. [[CrossRef](#)]
87. Peñas, J.R.V.; Zárte, J.M.; Khayet, M. Measurement of the thermal conductivity of nanofluids by the multi current hot-wire method. *J. Appl. Phys.* **2008**, *104*, 044314. [[CrossRef](#)]
88. Amin, A.-T.M.; Hamzah, W.A.W.; Oumer, A.N. Thermal conductivity and dynamic viscosity of mono and hybrid organic- and synthetic-based nanofluids: A critical review. *Nanotechnol. Rev.* **2021**, *10*, 1624–1661. [[CrossRef](#)]
89. Asadi, A.; Pourfattah, F.; Szilágyi, I.M.; Afrand, M.; Żyła, G.; Ahn, H.S.; Wongwisesi, S.; Nguyen, H.M.; Arabkoohsa, A.; Mahian, O. Effect of sonication characteristics on stability, thermophysical properties, and heat transfer of nanofluids: A comprehensive review. *Ultrason. Sonochem.* **2019**, *58*, 104701. [[CrossRef](#)]
90. Mahbulul, I.M.; Chong, T.H.; Khaleduzzaman, S.S.; Shahrul, I.M.; Saidur, R.; Long, B.D.; Amalina, M.A. Effect of Ultrasonication Duration on Colloidal Structure and Viscosity of Alumina-Water Nanofluid. American Chemical Society. *Ind. Eng. Chem. Res.* **2014**, *53*, 6677–6684. [[CrossRef](#)]